Whole-body Imaging of Adipose Tissues in Mouse at 9.4T

Patrick J Bolan[1], Amrutesh Puranik[2], John W Osborn Jr.[3], Maria Razzoli[3], Alessandro Bartolomucci[3], Pu Tzu Liu[4], Yi-Wei Lin[4], and Li-Na Wei[4]
[1]*Radiology - CMRR, University of Minnesota, Minneapolis, Minnesota, United States,* [2]*Mayo Clinic, Rochester, MN, United States,* [3]*Integrative Biology and Physiology, University of Minnesota, Minneapolis, MN, United States,* [4]*Pharmacology, University of Minnesota, Minneapolis, MN, United States*

Target Audience: Researchers using mouse models to study obesity and brown fat.

Purpose: High-resolution anatomical MRI is often used in murine studies of obesity and metabolism to help measure the amount of adipose tissue and its regional distribution in visceral and subcutaneous compartments (1,2). Several groups have also explored use of water-fat imaging (a.k.a. chemical-shift, or Dixon imaging) to help distinguish brown adipose tissue (BAT) from white adipose tissue (WAT), as BAT has both lower fat content and shorter T2* relaxation times than WAT (3,4). In this work, we sought to develop a adipose imaging protocol for post-mortem mouse imaging that provides both anatomical imaging and multiparametric water-fat imaging with very high spatial resolution (156 µm isotropic). Such acquisitions would allow for finer adipose tissue compartmentalization (e.g., interrenal vs. parametrial) and measurement of smaller BAT depots beyond the interscapular region.

Methods: All scans were performed using a 9.4T MRI system equipped with a 300mT/m gradient insert (Agilent, Santa Clara CA) and a mouse whole-body RF coil (Virtumed, Minneapolis MN). A total of 37 adult mice were imaged across three distinct research protocols investigating obesity-related metabolism. Mice were sacrificed 0.5-5 hours prior to scanning. Whole-body anatomical imaging was performed using a 3D T1-weighted fast spin echo (TR/TE=200/11ms, echo train length 16, echo spacing 5.4ms, matrix 1024x256x256, FOV 160x40x40mm, 156µm isotropic resolution, acquisition time ~14 min). Water-fat imaging was performed using a series of 3D gradient echo images with six evenly-spaced echo times (TR=10ms, TE=2.53-3.78ms, ΔTE=250µs, flip angle 5°, matrix 1024x256x256, FOV 160x40x40mm, 156µm isotropic resolution, acquisition time ~11 min per TE).

Reconstruction of water-fat imaging was performed in two steps. First, the shortest 3 TE values were reconstructed using the method of Berglund et al. (5) based on the implementation available in the ISMRM Fat-Water Toolbox v.1 (6). The lipid spectrum was modeled with a 9-component model proposed by Hamilton et al. (7). The 3-TE reconstruction, which did not include R2* relaxation, produced estimates of complex water (W), complex fat (F), and B0 offset frequency. Fat fraction maps were subsequently calculated as FF=abs(F)/((abs(F)+abs(W)). Secondly, an extended model that included R2* relaxtion was fit to all 6 TE values. Fits were performed independently for each pixel using a non-linear least squares curve fit. All image reconstructions were performed with Matlab; manual image segmentations were performed using Amira; adipose region nomenclature follows those of Vitali et al. (8).

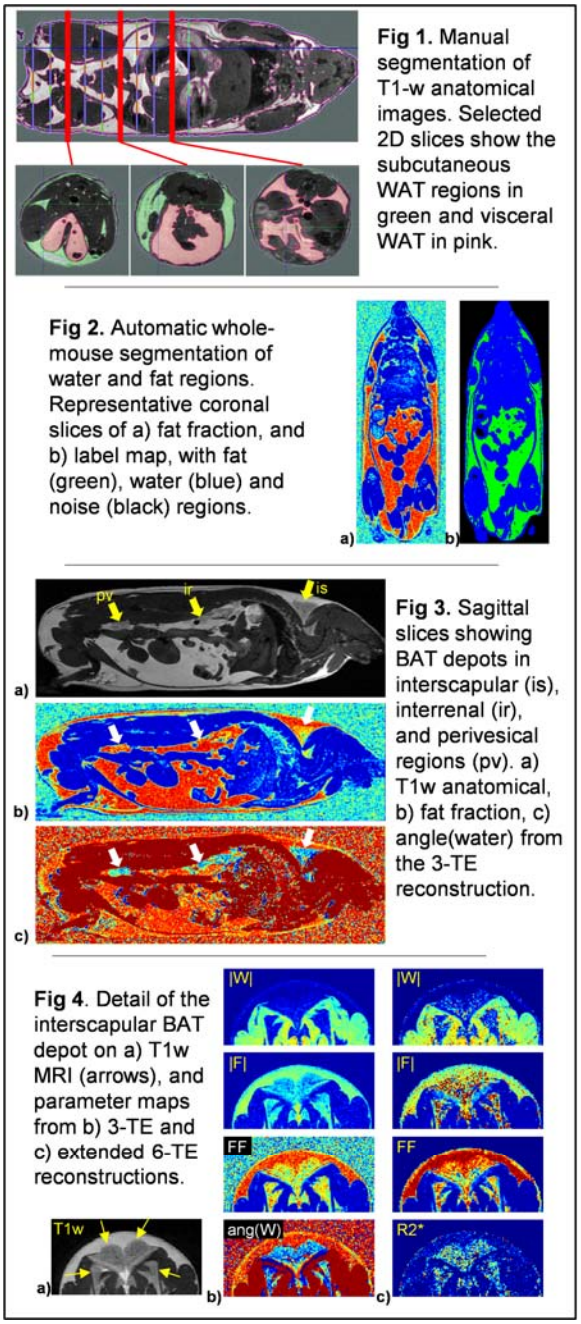

Fig 1. Manual segmentation of T1-w anatomical images. Selected 2D slices show the subcutaneous WAT regions in green and visceral WAT in pink.

Fig 2. Automatic whole-mouse segmentation of water and fat regions. Representative coronal slices of a) fat fraction, and b) label map, with fat (green), water (blue) and noise (black) regions.

Fig 3. Sagittal slices showing BAT depots in interscapular (is), interrenal (ir), and perivesical regions (pv). a) T1w anatomical, b) fat fraction, c) angle(water) from the 3-TE reconstruction.

Fig 4. Detail of the interscapular BAT depot on a) T1w MRI (arrows), and parameter maps from b) 3-TE and c) extended 6-TE reconstructions.

Results & Discussion: Both the T1-weighted anatomical images and the fat fraction images were suitable for segmenting adipose tissues. The T1-weighted images had relatively uniform signal from white adipose tissue and lower signal from other tissues, enabling high resolution manual segmentation of adipose tissue compartments (Fig.1). The fat fraction maps had the same spatial resolution and comparable SNR as the anatomical images, but have the advantage of a flatter profile and a more objective numeric interpretation. This can improve the robustness of both manual and automated segmentation analyses (1). As an example, Fig. 2 shows a slice from a whole-mouse water/fat/noise segmentation using only median filtering and thresholding operations.

Deposits of BAT in the interscapular and abdominopelvic regions could be identified on the T1-w anatomical images as fat regions with reduced signal intensity compared to WAT (Fig 3a). These regions generally exhibited a reduced fat fraction (Fig 3b), but were most distinct in the water phase maps (Fig 3c) from the 3-TE reconstruction. The results from the extended 6-TE reconstruction were noisier, but show reduced BAT/WAT contrast in the water, fat, and fat fraction maps. The BAT exhibited distinctly longer R2* values than WAT or muscle. These data suggest that the underlying R2* differences are confounded with water/fat composition in the 3-TE reconstruction. Note that these observations were consistent across all animals. Further work on the reconstruction technique is needed to incorporate lipid spectral variations (9) to better separate the mechanisms of BAT/WAT signal contrast and correct for potential T1 bias.

Conclusion: This work demonstrates anatomic and parametric water-fat imaging of adipose tissues in post mortem mice, with spatial resolution substantially higher than previous studies. This approach is applicable for finely-segmented quantitative volumetry of brown and white adipose tissue depots.

Acknowledgements: NIH P41 EB015894, P41 RR008079, R01 DK60621, and R21 CA179070, the W. M. Keck Foundation, and UMN AHC Translational Research Grant Program.

References: 1) Tang Y, et al., JMRI 2011 (34); 2) Bidar AW, et al., Am J Phys. Endo. Metab. 2012 (303); 3) Hu HH, et al., MRI 2012 (30); 4) Hu HH, et al., AJR 2013 (200); 5) Berglund J, et al., MRM 2010 (63); 6) Hu HH, et al., MRM 2012 (68); 7) Hamilton G, et al., NMR Biomed 2011 (24); 8) Vitali A, et al., J Lipid Res 2012 (53); 9) Hamilton G, et al., JMRI 2011 (34)